One-stage Contour Regression Network for Muscle Segmentation

Hongyuan Zhang[1], **Sijin Cai**[1,2], **Xiaofeng Wang**[3], **Yongjin Zhou**[1,2,*]

[1] School of Biomedical Engineering, Health Science Center, Shenzhen University, Shenzhen, China
[2]Marshall Laboratory of Biomedical Engineering, Shenzhen University, China
[3]School of Communication, Shenzhen University, Shenzhen, China
[*]The corresponding author: yjzhou@szu.edu.cn

Abstract

Muscle segmentation from ultrasound images is crucial for diagnosing and treating musculoskeletal diseases, as it provides geometric properties, such as area and thickness. However, most existing methods often rely on pixel-based segmentation networks to extract the muscle region. This is wasteful, inefficient, failing to meet the real-time requirements of dynamic analysis. Therefore, to address these issues, we introduce a novel **O**ne-stage **C**ontour-based **R**egression network, termed as **OCRSeg**, which formulates the muscle segmentation problem as contour regression in the vertical direction. In specific, we achieve this using a regression framework that is: 1) simple, consisting of an encoder for feature extraction and an MLP for regressing contour coordinates; 2) flexible, enforcing soft total variation constraints during training to ensure locally smooth muscle edges; and 3) optimized for band-like musculature. Extensive experimental results on two datasets demonstrate that our method outperforms other state-of-the-art segmentation methods in terms of accuracy and efficiency, achieving over 95.0% in mask IoU score and a FPS over 100 in running speed. Furthermore, another key advantage is that OCRSeg can achieve better clinical biometrics estimation compared with other techniques. We hope our proposed framework can serve as a fundamental and strong baseline for muscle segmentation task.

Introdution

Skeletal muscles, which are the muscle tissues in the human body, control movement and stabilize the skeleton (Zatsiorsky and Prilutsky 2012; Chen et al. 2015; Caresio et al. 2017). Accurate muscle segmentation is a prerequisite for implementing quantification analysis (Zhou et al. 2021; Caresio et al. 2017). The muscle region is crucial as it serves as the basis for subsequent qualitative assessments of area, angle and thickness, which provide clinical diagnosis information of the muscle condition of a patient and influence treatment planning decision (Cunningham et al. 2018). However, manual marking of target region is labor-intensive and time-consuming, and open to human bias and error (Darby et al. 2013). Here, automatic and accurate muscle segmentation has been a long-standing area with a great deal of need in clinical studies.

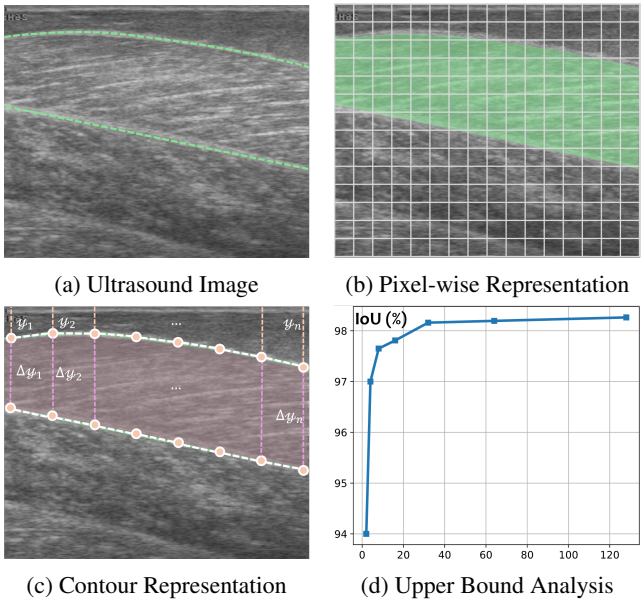

(a) Ultrasound Image (b) Pixel-wise Representation

(c) Contour Representation (d) Upper Bound Analysis

Figure 1: **Segmentation with different mask representations.** (a) is the original ultrasound image, where band-shaped muscle with annotated superficial and deep aponeurosis (green). (b) is the pixel-wise mask representation. (c) is our proposed contour representation. (d) is upper bound analysis. The 2d contour coordinates are sampled with Eq. 2. The higher the sampling number $\mathcal{N}$, the more detail is preserved. Even small settings yield good approximations of non-linear muscle shapes, and result is saturated with $\mathcal{N} = 128$.

The musculature are visible within B-mode ultrasound images and this imaging modality has been used to non-invasively quantify changes in muscle geometry during completion of different motor tasks (Darby et al. 2013; Zhou et al. 2021). Existing muscle segmentation techniques from ultrasound images can be categorized into three groups: 1) traditional methods, 2) pixel-based segmentation methods, and 3) contour-based segmentation methods. Traditional methods, which make strong assumptions about the shape of the observed aponeurosis, in particular, that they are straight (Zhou and Zheng 2008; Zhao and Zhang 2011), have

limited representation capabilities. Fortunately, with the development of deep learning, numerous pixel-based segmentation methods have been proposed, most of which mainly rely on U-shaped networks, such as U-Net (Ronneberger, Fischer, and Brox 2015), nnU-Net (Isensee et al. 2021), and TransUNet (Chen et al. 2024). DeeplabV3 (Chen 2017) is another commonly used segmentation framework due to the design of multi-scale perception. However, these methods all often result in significant resource consumption and necessitate additional post-processing.

In order to balance resource consumption, efficiency and performance, contour-based segmentation methods have increasingly attained researchers' attentions. They made a new starting point to tackle segmentation tasks through contour prediction methods. PolarMask (Xie et al. 2020) used polar contour descriptors to represent objects. Similarly, CPN (Upschulte et al. 2022) and FFPN (Chen et al. 2023) utilized Fourier descriptors to represent instance segmentation and achieved promising results. However, those methods' performance suffers from the low-quality of the center point or object detection. Point-Set (Wei et al. 2020) and PolySnake (Feng et al. 2024) used a point set to represent the contour and refines the initial rough contour through multiple steps of refinement operations. However, these solutions need to initialize the object contour and iteratively optimize to predict the final contour during inference, which needs a long running time. Thus, how to design an appropriate contour encoding method to represent muscle tissue regions is the key procedure for achieving real-time, accurate and low-resource segmentation.

In this study, we therefore present a one-stage contour-based segmentation framework, called *OCRSeg*, for muscle segmentation in ultrasound scans. Unlike prior paradigms, our proposed method models a band-shaped muscle as a set of uniformly sampled contour points and predicts the coordinates of contour points on the upper contour and the offsets between the lower contour, as shown in Figure 1c. OCRSeg is simple, easy to implement, and well-suited for practical medical scenarios. Briefly, our contributions are as follows:

- **Contour Representation:** In order to improve muscle tissue modeling, we design a simple contour representation and establish a connection between the contours for muscle segmentation. This design eliminates the need for additional post-processing and enables direct calculation of corresponding biometrics.
- **Optimized Biomedical Object Segmentation:** We propose a novel framework to segment muscle from ultrasound images. To the best of our knowledge, OCRSeg is the first one-stage approach with contour representation for muscle segmentation.
- **Superior Segmenation and Clinical Benefits:** The experimental results on two datasets demonstrate that our proposed method achieves better segmentation performance and offers greater clinical benefits compared to previous state-of-the-art techniques.

Method

Contour Representation

In this section, we first tackle the crucial challenge in contour-based segmentation methods: the representation of a single object. As described in the Introduction Section, we emphasize the importance of speed and avoiding post-processing issues in muscle segmentation. To address these concerns, we represent the band-shaped muscle contour $\mathcal{C}$ using uniformly sampled contour points of the upper and lower boundaries $\mathcal{C}_u$ and $\mathcal{C}_l$. As shown in Figure. 1c, the boundaries are extracted from the binary masks of images and uniformly divided into vertices with the same interval Δx. Assuming we perform $\mathcal{N}$ uniform sampling at the horizontal axis, the contour $\mathcal{C}$ is defined as:

$$\begin{aligned}\mathcal{C} &= \{\mathcal{C}_u, \mathcal{C}_l\} \\ &= \{\{y_1, y_2, .., y_{n-1}, y_n\}_u, \{y_1, y_2, .., y_{n-1}, y_n\}_l\}\end{aligned} \tag{1}$$

where $\{y_i\}_u, \{y_i\}_l$ denotes the coordinate of the i-th contour point y coordinate on the the superficial aponeurosis or deep aponeurosis. However, the superficial and deep aponeuroses are not independent, as they together form the upper and lower contour of the muscle. To capture this relationship, we regress the offset of the y coordinate from the deep aponeurosis to the superficial aponeurosis. Therefore, the final expressed contour $\mathcal{C}$ can be represented as:

$$\mathcal{C} = \{(y_1, \Delta y_1), (y_2, \Delta y_2)..., (y_{n-1}, \Delta y_{n-1}), (y_n, \Delta y_n)\} \tag{2}$$

where y_i represents the coordinate of a point on the superficial aponeurosis, and Δy_i represents the offset of that point from the deep aponeurosis to the superficial aponeurosis. This representation allows us to learn the connection between the superficial and deep aponeurosis, laying the foundation for muscle segmentation.

One-stage Contour Regression Network

The overall architecture of our proposed OCRSeg is illustrated in Figure 2. It has a backbone network and a regression head. The backbone network first takes ultrasound images as input to extract deep representations, and the regression head decodes the deep representations to regress contour points. In summary, the OCRSeg model can be expressed as:

$$f(I; \theta) = (\{(y_i, \Delta y_i)\}_{i=1}^{\mathcal{N}}) \tag{3}$$

where I is the input image and θ is the OCRSeg parameters.

Backbone: The backbone network aims to lessen the location information loss and gain more semantic deep representations through different receptive fields. Then those features will be input to the regression head. Our backbone is not limited to a specific network; we also compare existing convolution-based networks such as ResNet50 (He et al. 2016) and transformer-based networks like MiT (Xie et al. 2022) in Ablation Study Section.

Regression Head: The head consists of a MLP layer with $2\mathcal{N}$ outputs, being the outputs $1, ..., \mathcal{N}$ for superficial aponeurosis prediction and the output $\mathcal{N}+1, ..., 2\mathcal{N}$ for deep aponeurosis offsets. Once the predictions are obtained, it becomes effortless to reconstruct muscle region.

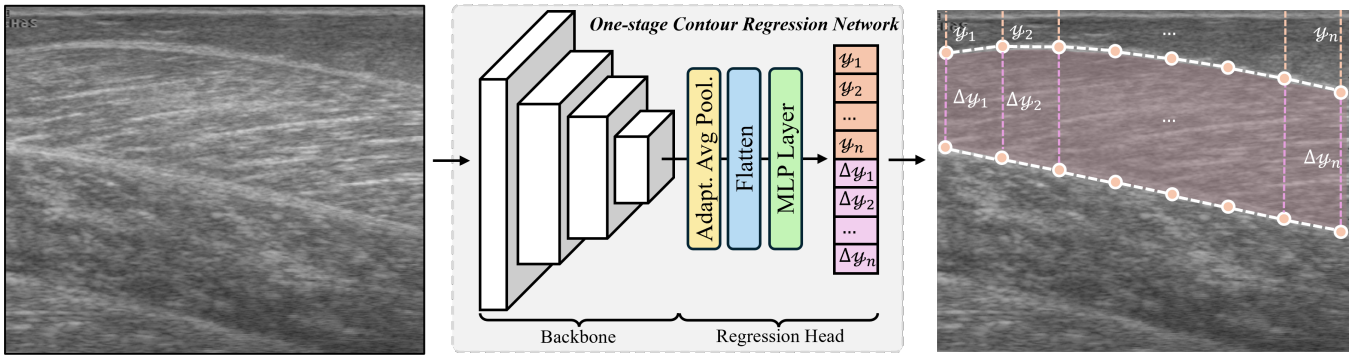

Figure 2: **Overview of our methodology.** The model takes an ultrasound image as input and outputs the coordinates of contour points on the superficial aponeurosis and the corresponding offsets for the deep aponeurosis.

Table 1: **Quantitative comparison results (mean ± std).** Comparison with other state-of-the-art methods on the MSeg dataset and FALLMUD dataset. The best results are highlighted in **bold**, and the second best results are underlined.

	Methods	Backbone	MSeg dataset		FALLMUD dataset		FPS ↑
			IoU (%) ↑	HD95 (pixel) ↓	IoU(%) ↑	HD95 (pixel) ↓	
Pixel-based	U-Net (Ronneberger, Fischer, and Brox 2015)	ResNet50	97.29 ± 1.99	2.31 ± 2.75	96.58 ± 1.37	4.08 ± 3.26	148.10
	UNet++ (Zhou et al. 2019)	ResNet50	**97.75 ± 0.78**	1.89 ± 1.59	**96.72 ± 0.80**	3.11 ± 1.96	124.95
	DeepLabv3+ (Chen et al. 2018)	ResNet50	96.87 ± 2.63	2.65 ± 2.76	94.72 ± 2.70	7.97 ± 4.33	151.31
	TransUNet (Chen et al. 2024)	ResNet50	97.70 ± 0.74	1.88 ± 1.43	96.62 ± 1.51	2.81 ± 1.94	66.52
	Swin-Unet (Cao et al. 2022)	Transformer	93.48 ± 2.16	4.76 ± 2.05	92.73 ± 1.82	6.16 ± 1.74	63.77
Contour-based	DeepHough (Zhao et al. 2021)	ResNet50	75.71 ± 11.29	20.62 ± 7.39	84.43 ± 3.98	5.97 ± 2.39	83.19
	PointSetAnchor (Wei et al. 2020)	ResNet50	93.12 ± 4.03	5.32 ± 3.48	91.83 ± 4.86	5.66 ± 2.51	103.53
	PolarMask (Xie et al. 2020)	ResNet50	95.53 ± 1.75	2.62 ± 0.38	94.15 ± 0.81	3.28 ± 0.45	122.49
	OCRSeg (Ours)	ResNet50	97.27 ± 0.23	**1.33 ± 0.38**	96.46 ± 0.73	2.27 ± 0.52	**197.92**
	OCRSeg (Ours)	Transformer	97.23 ± 0.36	1.37 ± 0.24	96.70 ± 0.63	**1.81 ± 0.53**	119.45

In addition, compared to segmentation networks that utilize encoder-decoder architecture, such as U-Net (Ronneberger, Fischer, and Brox 2015) and TransUNet (Chen et al. 2024), our proposed OCRSeg treats the segmentation problem as a regression task and only includes a single encoder. This design results in lower computational resource consumption and faster inference speed.

Regularization

Considering the physiological characteristics of muscles, the muscle edges, namely the aponeuroses, should be locally smooth. The total variation (Fatemi 1992) is a classical smooth regularization technique for image analysis. Inspired by this, we propose a new regularization $\mathcal{R}_{soft}$ term on the learning of edges by introducing a tolerance coefficient m, as follows:

$$\mathcal{R}_{soft} = \frac{1}{\mathcal{N}} \sum_{i \in \mathcal{N}} [abs(y_{i+1} - y_i) - m]_+ + [abs(\Delta y_{i+1} - \Delta y_i) - m]_+ \tag{4}$$

where $[u]_+ := max(0, u)$. m is a hyper-parameter representing a margin which controls how well we want the alignment to be. Following this procedure, we obtain a smooth edges of the muscle, while forgive small errors and maintain curvature. In this study, we empirically set $m = 0.02$.

Final Training Loss

In the training stage, we adopt the $\mathcal{L}_1$ loss, which is often used in coordinate regression tasks, to supervise the output coordinates and coordinate offsets.

$$\mathcal{L}_{final} = \mathcal{L}_1(y_{pred}, y_{true}) + \mathcal{L}_1(\Delta y_{pred}, \Delta y_{true}) + \mathcal{R}_{soft} \tag{5}$$

where y_{pred} and Δy_{pred} denote the predicted values for the coordinates and coordinate offsets, respectively, and y_{true} and Δy_{true} represent the corresponding ground truth values.

Experiment Protocol

Datasets

To evaluate our method, we conducted experiments using two datasets: the public dataset FALLMUD (Cunningham et al. 2018) and a private muscle segmentation dataset MSeg.

MSeg Dataset: This dataset consists of 40 subjects with a total of 1807 images. These images were captured using

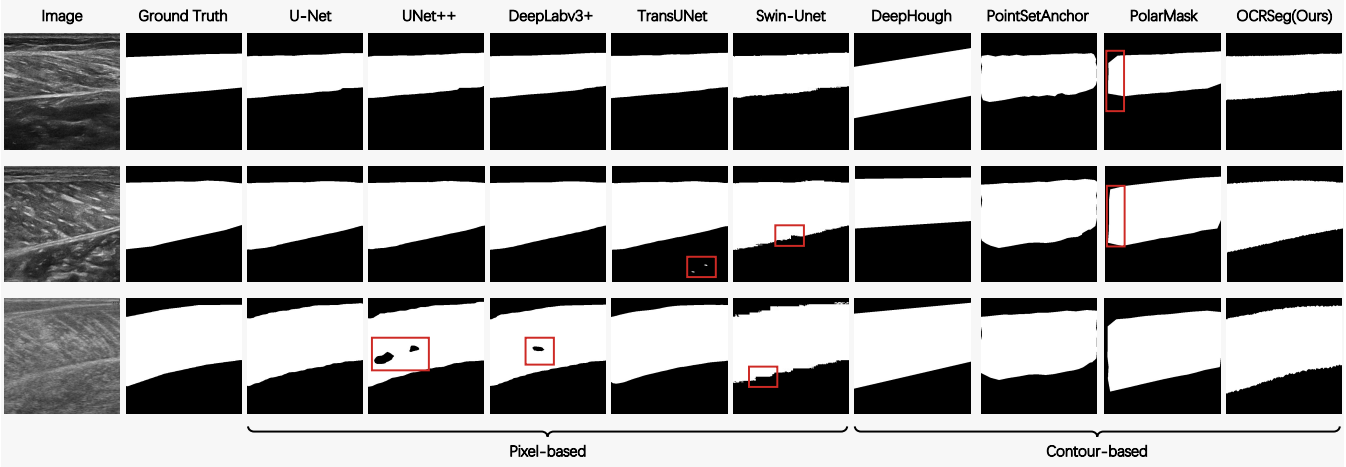

Figure 3: **Qualitative comparison results on sample test images from test set and independent set.** The top two rows represent the results of the test set of the MSeg dataset, and the bottom row represents the results of the FALLMUD dataset. Red rectangles highlight areas of interest where the segmentation performance is suboptimal.

a real-time B-mode ultrasonic scanner equipped with a 10 MHz electronic linear array probe. To avoid data leakage, we randomly divided the training and test sets at the subject-level. The training set comprises 1569 images from 35 subjects, while the test set contains 238 ultrasound images from 5 subjects. All images have a size of 512 $\times$ 512 pixels.

FALLMUD Dataset: This public dataset (Cunningham et al. 2018; Cronin 2020; Michard et al. 2021) comprises ultrasound images of calf muscles, designed for analyzing muscle weakness and preventing injuries. We used 504 standardized ultrasound images as an independent test set to further verify the generalization of the method. All images were recorded at 25 Hz from the calf muscles of 8 healthy volunteers during dynamic maximum isometric voluntary contractions. Image settings were constant across participants, and all images have been resized to 512 $\times$ 512 pixels.

Evaluation Metrics

Following the previous works (Cunningham et al. 2018; Upschulte et al. 2022; Chen et al. 2024), we adopt intersection over union (IoU) and 95% Hausdorff Distance (HD95) as evaluation metrics to assess the performance of our method. In addition, we also report the frames-per-second (FPS) as a speed-related metric.

Implementation Details

All experiments were implemented based on PyTorch's Python API (Paszke et al. 2019). Adam (Kingma and Ba 2014) was used as the optimizer with an initial learning rate of $5e^{-4}$ and a learning decay rate of 0.95 per epoch. We used *early-stop* mechanism on the test set in MSeg dataset to avoid over-fitting. For data augmentation, we adopted on-the-fly random mirroring and contrast adjustment strategies for all training data. Besides, all experiments were conducted on a single NVIDIA A800 GPU equipped with 80GB memory, alongside Intel(R) Xeon(R) Platinum 8358 CPUs.

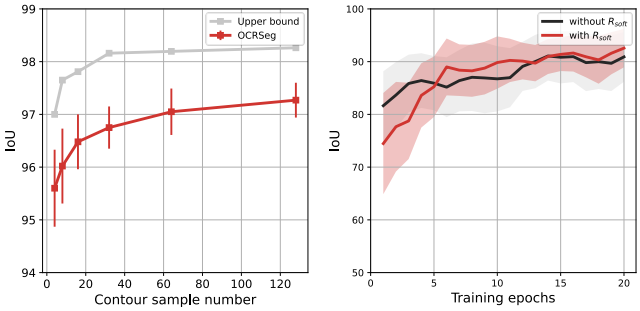

Figure 4: **Results of the ablation study. Left:** Performance of IoU score for different contour sample numbers $\mathcal{N}$ on MSeg dataset. **Right:** Comparison of test IoU scores with and without R_{soft}. As shown, OCRSeg with R_{soft} accelerates convergence and achieves a higher IoU score.

Main Results

Ablation Study

In this section, we conduct ablation experiments to analyze each module in OCRSeg. All models are based on ResNet50 backbone and MSeg dataset, unless otherwise noted.

The Number $\mathcal{N}$ of Contour Sampling: To determine the sampling number $\mathcal{N}$, we set $\mathcal{N} = \{4, 16, 32, 64, 128\}$ and evaluated the performance of the model under each setting. The IoU values for each setting are depicted in Figure 4. The results indicate that increasing the number of samples from 4 to 128 noticeably boosts the performance. This improvement is attributed to the enhanced expressiveness of the contour achieved by using a larger number of samples. Notably, when $\mathcal{N} = 128$, the IoU score exhibits the smallest standard deviation, indicating the model's stability. In addition, setting $\mathcal{N}$ to 128 incurs only a minor overhead compared to $\mathcal{N}$ or 16, as it primarily affects the fully connected output of the

final regression head. Based on these findings, We thus set $\mathcal{N} = 128$ in all our subsequent experiments to strike a favorable balance between performance and model compactness.

Regularization Effects: The results of R_{soft} regularization ablation experiment are illustrated in the Figure 4, which compares the IoU scores across training epochs with and without the R_{soft}. The black line represents performance without R_{soft}, while the red line shows performance with it. Initially, the model with R_{soft} exhibits lower performance due to the regularization's smoothing effects on muscle edges, causing it to take longer to adapt. However, as training progresses, the performance improves significantly, ultimately surpassing the model without R_{soft}. Besides, the shaded areas indicate standard deviation, demonstrating that the model with R_{soft} is more stable and exhibits less variability. These results highlight R_{soft}'s effectiveness in enhancing model performance and stability while ensuring smooth muscle edges and accommodating small errors.

Backbone Architecture: In addition, as shown in Table 1, we conducted an ablation study comparing two backbone networks: the CNN-based ResNet50 (He et al. 2016) and the Transformer-based MiT (Xie et al. 2022). Both architectures yielded similar results in terms of performance. This outcome can be attributed to our contour representation method, which effectively decouples the overall framework from the specific choice of backbone network. The framework demonstrates robust performance regardless of the underlying architecture, highlighting the flexibility of the method. For a fair comparison, we selected ResNet50 as our backbone to evaluate against other techniques.

Comparisons with the State-of-the-Art

We compared our method against other state-of-the-art (SOTA) approaches, including pixel-based segmentation models (U-Net (Ronneberger, Fischer, and Brox 2015), UNet++ (Zhou et al. 2019), Deeplabv3+ (Chen et al. 2018), TransUNet (Chen et al. 2024), Swin-Unet (Cao et al. 2022)) and contour-based segmentation models (DeepHough (Zhao et al. 2021), PointSetAnchor (Wei et al. 2020), PolarMask (Xie et al. 2020)). All models were meticulously trained and tested based on their official source code and parameters.

Quantitative Comparison: The quantitative results are reported in Table 1. As expected, our method yield a gain in performance over other contour-based methods on the MSeg dataset, with a mean IoU score and mean HD95 of 97.27 ± 0.23 and 1.33 ± 0.38 pixel respectively. This improvement can be attributed to the modeling based on upper and lower edges, which accommodates the shape variability and constraints of elongated muscle objects, leading to enhanced performance. Similarly, on the independent FALLMUD dataset, our proposed OCRSeg method performs best. Furthermore, the performance across both datasets indicates that OCRSeg shows better generalization and robustness compared to other contour-based methods. Compared to the pixel-based method, our approach achieves a slightly lower IoU score than the SOTA UNet++ (97.27 ± 0.23 *vs.* 97.75 ± 0.78). However, our method performs better on the HD95 metric (1.89 ± 1.59 *vs.* 1.33 ± 0.38).

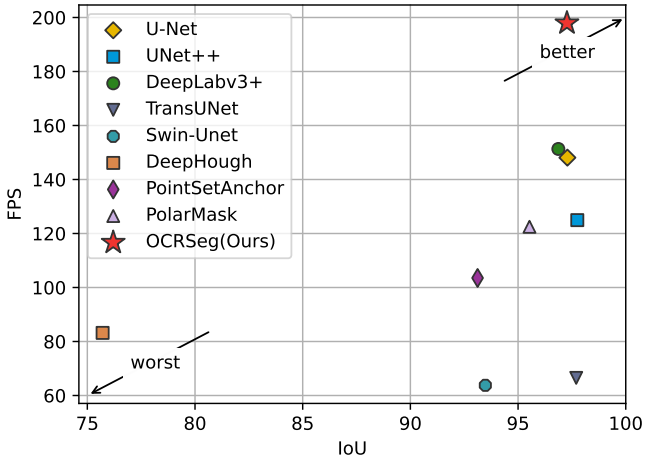

Figure 5: **The comparison of inference speed over different state-of-the-art methods on $MSeg$ dataset.** Better performance is indicated towards the top right.

Qualitative Comparison: We also present the qualitative comparison of the detection results in Figure 3, which clearly demonstrates that our method outperforms other methods. The pixel-based method often produces holes, abnormal segmentation results, or uneven edges. In contrast, our approach, which utilizes upper and lower contour representation, shows greater consistency with the ground truth. When compared to contour-based DeepHough, PolarMask, and PointAnchorSets, our results exhibit better muscle segmentation accuracy and reliability.

Inference Time Analysis: Results in Table 1 illustrate that our method is significantly faster than all other competitors with a very considerable margin. In addition, we also compared the relationship between model performance and running time. As illustrated in Figure 5, Our method, OCRSeg, demonstrates a favorable balance between accuracy and speed compared to other approaches.

Clinical Benefits

In this section, we analyze the usability of various methods in downstream clinical biometrics calculation tasks to evaluate their clinical benefits. Specifically, we selected UNet++, the top-performing pixel-based method, along with all contour-based methods for analysis and comparison.

Biometric Definition

We explored two common clinical metrics frequently used in practice: muscle thickness and aponeurosis length, which includes both superficial and deep aponeuroses. Each biometric is detailed below.

Muscle Thickness: The thickness (Caresio et al. 2017) is calculated by measuring the Euclidean distance between the

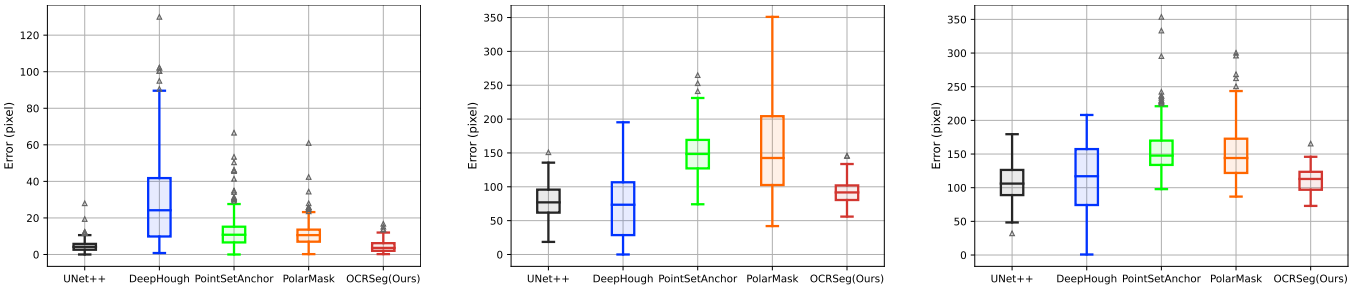

(a) Muscle Thinness (b) Superficial Aponeurosis Length (c) Deep Aponeurosis Length

Figure 6: **Box plots comparing the biometric measurement errors for U-Net++ and all contour methods, with distinct colors representing different methods.** (a) is muscle thickness, (b) and (c) are superficial and deep aponeurosis length.

endpoints of five segments between the two muscle aponeuroses at around 10%, 30%, 50%, 70% and 90% of the entire length of the muscle profile in the image. The final measurement was obtained as the average of these five distances. This metric is crucial for assessing muscle health and function, aiding in the diagnosis of conditions such as muscle atrophy (Caresio et al. 2017; Shi et al. 2007).

Aponeurosis Length: The aponeuroses consist of superficial and deep layers, as illustrated in Figure 1a. Aponeurosis length refers to the distance between the proximal and distal ends (Maganaris, Kawakami, and Fukunaga 2001). Accurate measurement of aponeurosis length is essential for understanding muscle mechanics and can provide insights into functional impairments or injuries (Evangelidis et al. 2015).

Error Analysis

The box-plot analysis (Williamson, Parker, and Kendrick 1989) was implemented to evaluate the agreement between the automatic and the manual measurement results. As shown in Figure 6, our proposed OCRSeg method demonstrates greater stability and fewer outliers across the three biometric measurements. In comparison to the pixel-based UNet++, the contour-based OCRSeg exhibits similar error rates but improved stability. In addition, due to our contour modeling approach, muscle thickness calculated using the OCRSeg method can be derived directly from the prediction results, while fascia length can be easily computed using the Euclidean distance formula. Unlike other methods, OCRSeg does not require additional post-processing steps, such as contour detection, thereby simplifying the workflow and making it more clinically friendly.

Conclusion

In this study, we introduced a novel one-stage method for muscle segmentation based on contour regression. Our proposed OCRSeg method offers simplicity and efficiency by eliminating the necessity for segmentation and post-processing, while still achieving competitive accuracy when compared to state-of-the-art methods. Furthermore, OCRSeg demonstrates improved consistency and stability in clinical biometric measurements. We believe that our approach has the potential to advance muscle morphological analysis and provide accurate measurements in various clinical and research settings.

References

Cao, H.; Wang, Y.; Chen, J.; Jiang, D.; Zhang, X.; Tian, Q.; and Wang, M. 2022. Swin-unet: Unet-like pure transformer for medical image segmentation. In *European conference on computer vision*, 205–218. Springer.

Caresio, C.; Salvi, M.; Molinari, F.; Meiburger, K. M.; and Minetto, M. A. 2017. Fully automated muscle ultrasound analysis (MUSA): Robust and accurate muscle thickness measurement. *Ultrasound in medicine & biology*, 43(1): 195–205.

Chen, C.; Yang, X.; Chen, R.; Yu, J.; Du, L.; Wang, J.; Hu, X.; Cao, Y.; Liu, Y.; and Ni, D. 2023. FFPN: Fourier Feature Pyramid Network for Ultrasound Image Segmentation. In *International Workshop on Machine Learning in Medical Imaging*, 166–175. Springer.

Chen, J.; Mei, J.; Li, X.; Lu, Y.; Yu, Q.; Wei, Q.; Luo, X.; Xie, Y.; Adeli, E.; Wang, Y.; et al. 2024. TransUNet: Rethinking the U-Net architecture design for medical image segmentation through the lens of transformers. *Medical Image Analysis*, 97: 103280.

Chen, L.-C. 2017. Rethinking atrous convolution for semantic image segmentation. *arXiv preprint arXiv:1706.05587*.

Chen, L.-C.; Zhu, Y.; Papandreou, G.; Schroff, F.; and Adam, H. 2018. Encoder-decoder with atrous separable convolution for semantic image segmentation. In *Proceedings of the European conference on computer vision (ECCV)*, 801–818.

Chen, X.; Li, Q.; Qi, S.; Zhang, H.; Chen, S.; and Wang, T. 2015. Continuous fascicle orientation measurement of medial gastrocnemius muscle in ultrasonography using frequency domain Radon transform. *Biomedical Signal Processing and Control*, 20: 117–124.

Cronin, N. 2020. *Automated analysis of musculoskeletal ultrasound images using deep learning*. Master's thesis.

Cunningham, R.; Sánchez, M. B.; May, G.; and Loram, I. 2018. Estimating full regional skeletal muscle fibre orientation from B-mode ultrasound images using convolutional,

residual, and deconvolutional neural networks. *Journal of Imaging*, 4(2): 29.

Darby, J.; Li, B.; Costen, N.; Loram, I.; and Hodson-Tole, E. 2013. Estimating skeletal muscle fascicle curvature from B-mode ultrasound image sequences. *IEEE Transactions on Biomedical Engineering*, 60(7): 1935–1945.

Evangelidis, P. E.; Massey, G. J.; Pain, M. T.; and Folland, J. P. 2015. Biceps femoris aponeurosis size: a potential risk factor for strain injury? *Medicine & Science in Sports & Exercise*, 47(7): 1383–1389.

Fatemi, O. E. 1992. Nonlinear total variation based noise removal algorithms. *Physica D: Nonlinear Phenomena*.

Feng, H.; Zhou, K.; Zhou, W.; Yin, Y.; Deng, J.; Sun, Q.; and Li, H. 2024. Recurrent generic contour-based instance segmentation with progressive learning. *IEEE Transactions on Circuits and Systems for Video Technology*.

He, K.; Zhang, X.; Ren, S.; and Sun, J. 2016. Deep residual learning for image recognition. In *Proceedings of the IEEE conference on computer vision and pattern recognition*, 770–778.

Isensee, F.; Jaeger, P. F.; Kohl, S. A.; Petersen, J.; and Maier-Hein, K. H. 2021. nnU-Net: a self-configuring method for deep learning-based biomedical image segmentation. *Nature methods*, 18(2): 203–211.

Kingma, D. P.; and Ba, J. 2014. Adam: A method for stochastic optimization. *arXiv preprint arXiv:1412.6980*.

Maganaris, C. N.; Kawakami, Y.; and Fukunaga, T. 2001. Changes in aponeurotic dimensions upon muscle shortening: in vivo observations in man. *The Journal of Anatomy*, 199(4): 449–456.

Michard, H.; Luvison, B.; Pham, Q.-C.; Morales-Artacho, A. J.; and Guilhem, G. 2021. AW-Net: Automatic muscle structure analysis on B-mode ultrasound images for injury prevention. In *Proceedings of the 12th ACM Conference on Bioinformatics, Computational Biology, and Health Informatics*, 1–9.

Paszke, A.; Gross, S.; Massa, F.; Lerer, A.; Bradbury, J.; Chanan, G.; Killeen, T.; Lin, Z.; Gimelshein, N.; Antiga, L.; et al. 2019. Pytorch: An imperative style, high-performance deep learning library. *Advances in neural information processing systems*, 32.

Ronneberger, O.; Fischer, P.; and Brox, T. 2015. U-net: Convolutional networks for biomedical image segmentation. In *Medical image computing and computer-assisted intervention–MICCAI 2015: 18th international conference, Munich, Germany, October 5-9, 2015, proceedings, part III 18*, 234–241. Springer.

Shi, J.; Zheng, Y.-P.; Chen, X.; and Huang, Q.-H. 2007. Assessment of muscle fatigue using sonomyography: Muscle thickness change detected from ultrasound images. *Medical engineering & physics*, 29(4): 472–479.

Upschulte, E.; Harmeling, S.; Amunts, K.; and Dickscheid, T. 2022. Contour proposal networks for biomedical instance segmentation. *Medical image analysis*, 77: 102371.

Wei, F.; Sun, X.; Li, H.; Wang, J.; and Lin, S. 2020. Point-set anchors for object detection, instance segmentation and pose estimation. In *Computer Vision–ECCV 2020: 16th European Conference, Glasgow, UK, August 23–28, 2020, Proceedings, Part X 16*, 527–544. Springer.

Williamson, D. F.; Parker, R. A.; and Kendrick, J. S. 1989. The box plot: a simple visual method to interpret data. *Annals of internal medicine*, 110(11): 916–921.

Xie, E.; Sun, P.; Song, X.; Wang, W.; Liu, X.; Liang, D.; Shen, C.; and Luo, P. 2020. Polarmask: Single shot instance segmentation with polar representation. In *Proceedings of the IEEE/CVF conference on computer vision and pattern recognition*, 12193–12202.

Xie, Y.; Zhang, J.; Xia, Y.; and Wu, Q. 2022. Unimiss: Universal medical self-supervised learning via breaking dimensionality barrier. In *European Conference on Computer Vision*, 558–575. Springer.

Zatsiorsky, V. M.; and Prilutsky, B. I. 2012. *Biomechanics of skeletal muscles*. Human Kinetics.

Zhao, H.; and Zhang, L.-Q. 2011. Automatic tracking of muscle fascicles in ultrasound images using localized radon transform. *IEEE transactions on biomedical engineering*, 58(7): 2094–2101.

Zhao, K.; Han, Q.; Zhang, C.-B.; Xu, J.; and Cheng, M.-M. 2021. Deep hough transform for semantic line detection. *IEEE Transactions on Pattern Analysis and Machine Intelligence*, 44(9): 4793–4806.

Zhou, Y.; and Zheng, Y.-P. 2008. Estimation of muscle fiber orientation in ultrasound images using revoting hough transform (RVHT). *Ultrasound in medicine & biology*, 34(9): 1474–1481.

Zhou, Y.; Zheng, Y.-P.; Zhou, Y.; and Zheng, Y.-P. 2021. Measurement of Skeletal Muscle Fascicle Length. *Sonomyography: Dynamic and Functional Assessment of Muscle Using Ultrasound Imaging*, 79–91.

Zhou, Z.; Siddiquee, M. M. R.; Tajbakhsh, N.; and Liang, J. 2019. Unet++: Redesigning skip connections to exploit multiscale features in image segmentation. *IEEE transactions on medical imaging*, 39(6): 1856–1867.